Multiple Beam Synthesis of Passively Cooled 5G Planar Arrays Using Convex Optimization

Aslan, Yanki; Puskely, Jan; Roederer, Antoine; Yarovoy, Alexander

DOI
10.1109/TAP.2019.2955885

Publication date
2019

Document Version
Final published version

Published in
IEEE Transactions on Antennas and Propagation

Multiple Beam Synthesis of Passively Cooled 5G Planar Arrays Using Convex Optimization

Yanki Aslan, *Graduate Student Member, IEEE*, Jan Puskely, Antoine Roederer, *Life Fellow, IEEE*, and Alexander Yarovoy, *Fellow, IEEE*

***Abstract*— An extended-feature, system-driven convex algorithm for the synthesis of uniform-amplitude, irregular planar phased arrays with simultaneous multi-beam optimization for mm-wave 5G base station applications in multi-user scenarios is presented. The inter-user interferences are suppressed by minimizing the maximum sidelobe level (SLL) for a beam scanned freely inside a given sector. The aperture size is restricted to the size of the heatsink baseplate dimensions. A minimum guaranteed inter-element spacing in the final layout is pre-defined, which prevents element overlapping, eases the thermal problem and helps reduce the effects of high mutual coupling (MC). The algorithm performance is tested via the synthesis of a 64-element integrated array with at least half a wavelength inter-element spacing. The optimized array results show that, compared to their regular counterparts, significant reduction in the SLLs is achieved for a beam scanned inside the defined sector, while keeping the maximum temperature of the array at a reliable level. The effect of MC on the results is also investigated via full-wave simulations and it is explained how embedded element patterns can potentially be included in the optimization. Superior capabilities of the proposed method are illustrated by comparing the algorithm output to those reported in the state-of-the-art literature.**

***Index Terms*— Antenna synthesis, convex optimization, fifth generation (5G), irregular antenna array, multibeam optimization (MBO), passive cooling, space tapering.**

I. Introduction

THE 5G communication systems are expected to achieve approximately 1000× communication capacity growth and less than 1 ms latency in transferred data while supporting massive Internet of Things [1], [2]. To realize the throughput metrics of 5G, a vast amount of spectrum is necessary, which is available in the mm-wave bands. Despite the advantage of large bandwidth, transmissions at mm-wave frequencies have significantly less favorable RF link budgets if antenna gains are not increased [3], as well as much reduced power amplifier efficiencies [4], [5] lead to increased heat dissipation.

Manuscript received February 19, 2019; revised November 7, 2019; accepted November 21, 2019. Date of publication December 9, 2019; date of current version May 5, 2020. This work was supported in part by Netherlands Organisation for Scientific Research (NWO) and in part by NXP Semiconductors in the framework of the program on Advanced 5G Solutions—Antenna Topologies and Front-end Configurations for Multiple Beam Generation. *(Corresponding author: Yanki Aslan.)*

The authors are with the Microwave Sensing Signals and Systems Group, Department of Microelectronics, Delft University of Technology, 2600 Delft, The Netherlands (e-mail: y.aslan@tudelft.nl; j.puskely-1@tudelft.nl; a.g.roederer@tudelft.nl; a.yarovoy@tudelft.nl).

Color versions of one or more of the figures in this article are available online at http://ieeexplore.ieee.org.

Digital Object Identifier 10.1109/TAP.2019.2955885

This heat excess has to be removed to maintain a safe and reliable operation at the base station antenna array. However, small wavelengths results in high packaging densities of the front-ends and makes integration of the sub-systems with a cooling structure a major issue, especially with one amplifier per element [6]. On the other hand, strict cost and energy requirements of 5G transmitters require the use of simple, passive cooling strategies.

The problem of cooling of electronics under a conduction-dominated cooling scenario was studied in [7] by solving the heat equation in 2-D and optimizing the positions of the heat sources inside an aperture depending on the position of the heatsink. Combining such an approach mathematically with the array factor and thus the radiation pattern of the array (by assuming the antennas are at the same 2-D location with the heat-generating transceiver chips) would result in a "joint" optimization of both thermal and electromagnetic performances. Traditionally, conduction-based thermal management is applied in conventional phased arrays where electronic circuit cards are placed orthogonally to the array and the cooling is achieved from the outer edges of the array via a large heatsink [8]. For such systems, intuitively, it can be inferred that more elements (chips) should be placed at the edges of the aperture since otherwise, the heat gets trapped in the middle of the array. However, as explained in [9], such traditional arrays are not preferred in 5G since they are incompact and they need a large number of RF boards with additional cabling for signal routing. What industry prefers today for 5G is a single, multi-layer RF board antenna that is low-cost and low-profile. In such designs, the radiators are placed on one side of the board while the chips are located on the opposite side where the heatsink is attached. The dominating cooling mechanism in this case becomes the natural convection to the third dimension instead of the conduction in 2-D toward the array edges since the heat is not trapped anymore, but is directly transferred to the heatsink and finally to the surrounding air. Thermal modeling of such systems is done via thermal resistors representing the temperature difference among different contact points (board node, chip case, solder bumps etc.) in the design along the third dimension [10], which decouples the thermal and electromagnetic aspects in terms of the element positions. The only practice in this case for an antenna array topology designer is to artificially imply thermal-awareness in the 2-D element optimization procedure by putting smart constraints

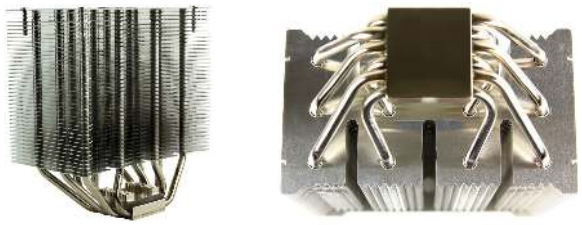

(a) (b)

Fig. 1. Sample passive CPU cooler and Mugen MAX from Scythe EU GmbH [11]. (a) Side view of the heatsink. (b) Baseplate and heat pipes.

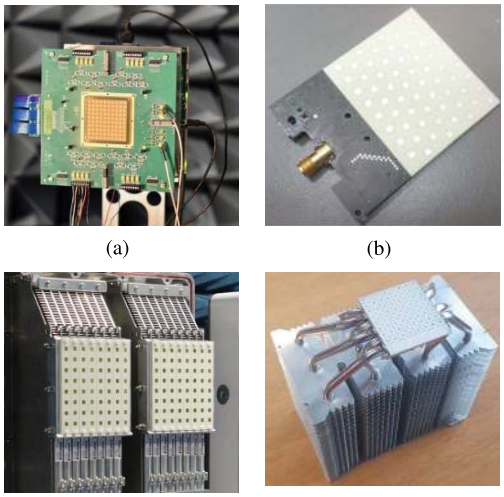

(a) (b) (c) (d)

Fig. 2. 5G state-of-the-art active integrated phased base station antenna arrays from the industry. (a) IBM [13]. (b) Nokia Bell Labs [14]. (c) Ericsson [15]. (d) NXP semiconductors [16].

in the electromagnetic optimization, which are defined by the specifications of the heatsink.

In 5G, as suggested in [9], the commercially available, low-cost and reliable passive CPU coolers with large heat removal capabilities can directly be used for cooling by attaching the transceiver chips to the baseplate of the cooler. An example of a standard CPU cooler [11] is given in Fig. 1.

In fact, such coolers can be efficiently used in densely spaced regular array layouts at mm-waves with a double-sided antenna design having the radiators on one side and beamforming chips and heatsink on the other side. However, high expectations for 5G require sufficient simultaneous frequency re-use through formation of multiple beams with low interference and thus with low side lobes (the concept of space-division multiple access (SDMA) [12]). The maximum sidelobe level (SLL) of the regular layouts (which is around -13 dB) contradicts with this requirement. On the other hand, such regular arrays are currently proposed in the very recent 5G (Massive) MIMO base stations by the leading organizations such as IBM [13], Nokia Bell Labs [14], Ericsson [15], and NXP Semiconductors [16] (see Fig. 2).

Therefore, it is important for the antenna community to synthesize novel irregular array layouts that have lower SLLs in the field of view and are compatible with the cooling systems. Besides, it was shown that irregular arrays with larger than half-wavelength inter-element spacing can bring further passive cooling due to the increased substrate-to-air surface area around each element [9]. This provides an additional superiority of irregular layouts with controlled minimum element spacing over the traditional regular half a wavelength spaced arrays. However, it is worth noting that the work in [9] was an initial study to explain that 5G antenna design requires a multidisciplinary work considering the thermal and electromagnetic aspects. There was no smart optimization technique applied to find out the best positions of elements for 5G SDMA. The baseplate dimension restriction of the CPU cooler was also ignored in the element placement, which will lead to a requirement on high-cost special design of an optimal heatsink for each array.

From the discussion above, it is clear that there is a necessity to consider both the thermal aspects (power efficiency, integration with the standard commercially-available low-cost cooling systems, etc.) and the electromagnetic aspects (minimum required gain, required scan range, maximum tolerable SLL and interference, etc.) when designing chip-integrated 5G antennas.

In the literature on antenna (or chip) array topology optimization, being motivated by the practicality and optimum power efficiency of uniformly excited arrays [17], many uniform amplitude array synthesis techniques have been proposed that are based on global optimization [18]–[20] and deterministic [21], [22] methods. It was shown that computational burden in global optimization increases rapidly with the number of array elements and the optimality of the solution is not guaranteed. Although deterministic methods are much more efficient, it was found out that they require the *a priori* knowledge of a reference (and ideally optimal) continuous source to be emulated. Recently, iterative convex optimization has been introduced for the synthesis of equi-amplitude arrays as a relatively efficient and powerful alternative [23], [24].

In convex optimization for planar array synthesis, defining a minimum inter-element spacing for the final layout is more challenging compared to the linear case [25] and, if ignored, the designed array elements may have quite small spacings ($<0.3\lambda$), as obtained in [23] and [26]. In addition to the thermal problem, this may lead to very high mutual coupling (MC) levels or even an unrealizable design. An effort was made in [27] to force a minimum inter-spacing by defining a circle around each element in which the total selection weight of the elements cannot exceed one. However, since any element could be selected with a weight less than 0.5, there is no guarantee that the spacing would be kept at the desired value. In [24], the minimum spacing control was applied in between the concentric circular rings, which can actually be represented as a 1-D constraint similar to the linear array case. In [28], convex optimization was combined with the method of perturbed compressive sampling (PCS) to give a constraint to the inter-element spacing in a free 2-D space with no forced symmetry. Nevertheless, the synthesized arrays were power-inefficient due to the large-scale amplitude tapering. In [29], Chaotic particle swarm optimization (PSO) technique was efficiently applied to synthesize uniformly excited arrays

TABLE I

CHARACTERISTICS OF THE PROPOSED APPROACH IN COMPARISON TO THE STATE-OF-THE-ART METHODS

	Uniform amplitude excitation	Pre-defined min. element spacing	Multi-beam optimization	Computation efficiency	5G SDMA compatibility
Ref. [19]	✓	✓	×	Low	×
Ref. [20]	×	✓	✓	Low	×
Ref. [21]	✓	×	×	High	×
Ref. [22]	✓	✓	×	High	×
Ref. [23]	✓	×	×	Moderate	×
Ref. [24]	✓	✓	×	Moderate	×
Ref. [27]	×	✓	×	Moderate	×
Ref. [28]	×	✓	×	Moderate	×
Ref. [29]	✓	✓	×	Low	×
Ref. [30]	×	×	✓	Moderate	×
Ref. [31]	×	×	✓	Moderate	×
This method	✓	✓	✓	Moderate	✓

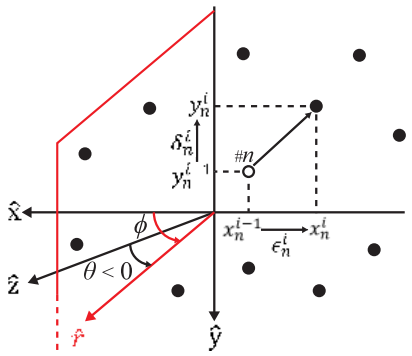

Fig. 3. Schematic of the planar array, coordinate system, and notations. θ is the elevation angle defined as the angle between the observation direction $\hat{r}$ and $\hat{z}$. A vertical plane is shown in red which includes the vector $\hat{r}$ and its projection onto the $\hat{x}\hat{y}$ plane. ϕ is the azimuth angle defined as the angle between this vertical plane and $\hat{x}$.

with a pre-defined minimum inter-spacing. However, the aim was to maximize the power collected by a receiving rectenna and the maximum allowed SLL was defined as a constraint, which is not minimized. Besides, the effect of beam scanning was not taken into account during the optimization in the above-mentioned methods.

Multi-beam optimization (MBO) was recently introduced in [20], [30], and [31] and it was shown that simultaneous parameter optimization for the broadside and the outermost scanned beams is necessary to guarantee that the SLL everywhere in the visible region will be less than the minimized SLL when the beam is scanned in a defined sector. In 5G, an array topology optimized via MBO will perform statistically the best in terms of the inter-user interference among the SDMA users sharing the same time and frequency resources. However, in the presented MBO literature, amplitude tapering with a large dynamic range was applied and there was no control on the spacing between the elements, which are two undesired features resulting from the sparsity-based nature of the proposed algorithms.

In this article, we propose the first optimization technique which simultaneously: 1) formulates the array topology optimization problem in an advance way (i.e. system-based optimization to achieve certain system performance within the angular sector statistically, while systematically approaching the thermal issues); 2) uses the same (or more advanced) optimization algorithm than any previously published article; 3) applies more advanced optimization constraints than any previously published article; 4) results in 2-D array topologies with electromagnetic and thermal performances better than any previously published; 5) is able to take into account MC of the elements in natural way; and 6) is computationally efficient.

The superiority of the proposed approach as compared to the state-of-the-art literature is summarized in Table I. The thermal analyses in [9], which were tested for several existing irregular array topologies (spiral arrays, thinned arrays, circular ring arrays, etc.), are also performed for the proposed sector-specific optimized layout. As per authors' knowledge, none of the earlier studies have combined interference-awareness (via multi-beam SLL minimization in a pre-defined cell sector) and thermal-awareness (via uniform amplitudes and pre-defined aperture size and minimum element spacing) with an efficient and easy-to-solve optimization algorithm.

The major contributions of this article are listed as follows.

1) Practical, 5G SDMA application specific integrated system design challenges and limitations in array topology optimization are discussed for the first time, with useful insights and recommendations.
2) A novel, extended-feature array synthesis method with possiblities to have uniform-amplitude excitations, simultaneous MBO, inter-element spacing and aperture size restriction and MC inclusion via embedded element pattern simulation is introduced using a low analytical complexity, easy-to-solve and relatively efficient convex optimization technique.
3) A novel convex formulation of the minimum inter-element spacing constraint in planar arrays with no forced symmetry is proposed.
4) The radiation pattern performance of the optimal space-tapered arrays in a 5G SDMA system is studied for the first time under a typical 5G base station deployment scenario.
5) The effect of array's integration with the commercially available, standard, passive CPU cooling modules on the electromagnetic optimization consraints and the resulting radiation and cooling performance is investigated for the first time.
6) As compared to the outcome of the techniques presented in the state-of-the-art literature, competitive or better radiation pattern and, in general, system performances are obtained using the proposed method with increased 5G SDMA compatibility.

The rest of this article is organized as follows. The optimization problem is formulated in Section II. The synthesis results are presented in Section III. Section IV concludes this article.

II. FORMULATION OF THE OPTIMIZATION PROBLEM

Let us consider an N-element uniformly excited planar array, as shown in Fig. 3 with the coordinate system and notations used throughout this article.

If the magnitude of the field is equated to one toward broadside as in [23], the far-field radiated by such an array is given by

$$f(\theta,\phi)=\frac{1}{N}\sum_{n=1}^{N}E_n(\theta,\phi)e^{jk(x_n\sin\theta\cos\phi+y_n\sin\theta\sin\phi)} \quad (1)$$

where $E_n(\theta)$ is the embedded pattern of the nth element. If the same isolated pattern, $E(\theta,\phi)$ is assumed for each element for simplicity, the far-field, $f(\theta,\phi)$ becomes

$$f(\theta,\phi)=\frac{E(\theta,\phi)}{N}\sum_{n=1}^{N}e^{jk(x_n\sin\theta\cos\phi+y_n\sin\theta\sin\phi)}. \quad (2)$$

As proposed in [23], the iterative optimization technique is applied by starting from a uniformly distributed array and moving the nth element by ϵ_n^i in the $\hat{\mathrm{x}}$ and δ_n^i in the $\hat{\mathrm{y}}$-direction at the ith step of the algorithm, which gives

$$x_n^i=x_n^{i-1}+\epsilon_n^i,\quad y_n^i=y_n^{i-1}+\delta_n^i. \quad (3)$$

As previously realized in [23], the far-field expression in (2) can be linearized around the element locations using the Taylor expansion when the following relations hold:

$$\left|k\sin\theta\cos\phi(\epsilon,\delta)_n^i\right|\ll 1,\ \text{i.e.,}\ \left|(\epsilon,\delta)_n^i\right|\ll\lambda/2\pi=0.16\lambda. \quad (4)$$

In this case, the far-field at the ith iteration can be approximated by

$$f_{\epsilon_n,\delta_n}^i(\theta,\phi)\approx\frac{E(\theta,\phi)}{N}\sum_{n=1}^{N}e^{jk\left(x_n^{i-1}\sin\theta\cos\phi+y_n^{i-1}\sin\theta\sin\phi\right)}\times\left(1+jk\epsilon_n^i\sin\theta\cos\phi\right)\left(1+jk\delta_n^i\sin\theta\sin\phi\right). \quad (5)$$

If the sufficiently small high-order terms in (5) are ignored to keep the convexity of the problem, the far-field becomes

$$f_{\epsilon_n,\delta_n}^i(\theta,\phi)\approx\frac{E(\theta,\phi)}{N}\sum_{n=1}^{N}e^{jk\left(x_n^{i-1}\sin\theta\cos\phi+y_n^{i-1}\sin\theta\sin\phi\right)}\times\left(1+jk\epsilon_n^i\sin\theta\cos\phi+jk\delta_n^i\sin\theta\sin\phi\right). \quad (6)$$

Assume that the beam is scanned at p different angles where $(\theta_{s_m},\phi_{s_m})$ represents the direction of maximum radiation for the scanned beam $s_{m=1,2,\ldots,p}$. In such a scenario, the phase shift of the nth element for the scan angle $(\theta_{s_m},\phi_{s_m})$ at the ith iteration is given by

$$\Phi_{n,s_m}^i=e^{-jk\left(x_n^i\sin\theta_{s_m}\cos\phi_{s_m}+y_n^i\sin\theta_{s_m}\sin\phi_{s_m}\right)}. \quad (7)$$

Following similar steps, the far-field expression in (6) can be modified to take into account the effect of scanning via multiplication with (7). Thus, the far-field of a scanned beam s_m at the ith iteration can be computed as follows:

$$\begin{aligned}f_{\epsilon_n,\delta_n}^{i,s_m}(\theta,\phi)\approx\ &\frac{E(\theta,\phi)}{N}\sum_{n=1}^{N}e^{jkx_n^{i-1}(\sin\theta\cos\phi-\sin\theta_{s_m}\cos\phi_{s_m})}\\&\times e^{jky_n^{i-1}(\sin\theta\sin\phi-\sin\theta_{s_m}\sin\phi_{s_m})}\\&\times\left(1+jk\epsilon_n^i(\sin\theta\cos\phi-\sin\theta_{s_m}\cos\phi_{s_m}\right)\\&+jk\delta_n^i(\sin\theta\sin\phi-\sin\theta_{s_m}\sin\phi_{s_m})). \quad (8)\end{aligned}$$

If the u-v coordinates are introduced as

$$\begin{aligned}u&=\sin\theta\cos\phi,\quad u_{s_m}=\sin\theta_{s_m}\cos\phi_{s_m}\\v&=\sin\theta\sin\phi,\quad v_{s_m}=\sin\theta_{s_m}\sin\phi_{s_m}\end{aligned} \quad (9)$$

the field expression in (8) can be rewritten as

$$f_{\epsilon_n,\delta_n}^{i,s_m}(u,v)\approx\frac{E(u,v)}{N}\sum_{n=1}^{N}e^{jk\left(x_n^{i-1}(u-u_{s_m})+y_n^{i-1}(v-v_{s_m})\right)}\times\left(1+jk\epsilon_n^i(u-u_{s_m})+jk\delta_n^i(v-v_{s_m})\right). \quad (10)$$

The vectors of parameters in the algorithm are defined as

$$\begin{aligned}\boldsymbol{x}^i&=\begin{bmatrix}x_1^i&\cdots&x_N^i\end{bmatrix}^T,\quad \boldsymbol{y}^i=\begin{bmatrix}y_1^i&\cdots&y_N^i\end{bmatrix}^T\\\boldsymbol{\epsilon}^i&=\begin{bmatrix}\epsilon_1^i&\cdots&\epsilon_N^i\end{bmatrix}^T,\quad \boldsymbol{\delta}^i=\begin{bmatrix}\delta_1^i&\cdots&\delta_N^i\end{bmatrix}^T\\\boldsymbol{u_s}&=\begin{bmatrix}u_{s_1}\cdots u_{s_p}\end{bmatrix},\quad \boldsymbol{v_s}=\begin{bmatrix}v_{s_1}&\cdots&v_{s_p}\end{bmatrix}\\(\boldsymbol{U},\boldsymbol{V})_{\boldsymbol{SL},\boldsymbol{s}}&=\begin{bmatrix}(\boldsymbol{u},\boldsymbol{v})_{\boldsymbol{SL},\boldsymbol{s_1}}&\cdots&(\boldsymbol{u},\boldsymbol{v})_{\boldsymbol{SL},\boldsymbol{s_p}}.\end{bmatrix}\end{aligned} \quad (11)$$

In (11), $\boldsymbol{x}^i$ and $\boldsymbol{y}^i$ contain the element locations. $\boldsymbol{\epsilon}^i$ and $\boldsymbol{\delta}^i$ contain the position shifts in the $\hat{\mathrm{x}}$- and $\hat{\mathrm{y}}$-directions at the ith iteration, respectively. Scan angles used in the optimization form $\boldsymbol{u_s}$ and $\boldsymbol{v_s}$. $(\boldsymbol{U},\boldsymbol{V})_{\boldsymbol{SL},\boldsymbol{s_m}}$ is a vector containing the (u,v) values forming the sidelobe region for each scan angle, s_m. These regions are determined according to a pre-specified main beam radius, r_b, such that

$$(u,v)\in(\boldsymbol{u},\boldsymbol{v})_{\boldsymbol{SL},\boldsymbol{s_m}}\ if\ (u-u_{s_m})^2+(v-v_{s_m})^2>r_b^2. \quad (12)$$

Furthermore, in order to guarantee a pre-defined minimum inter-element spacing $d_{\min}$ in the final layout, the spacing between each element pair (α,β) is forced to be larger than $d_{\min}$ at each iteration

$$\left(x_\alpha^i-x_\beta^i\right)^2+\left(y_\alpha^i-y_\beta^i\right)^2\geq d_{\min}^2. \quad (13)$$

The constraint in (13) is non-convex since a convex expression on the left-hand side of the inequality is forced to be larger than a real constant. Recall that the positions of the nth element at the ith iteration of the algorithm are given by (3). Considering that $(\epsilon_{\alpha,\beta}^i)^2$, $(\delta_{\alpha,\beta}^i)^2$, $(\epsilon_\alpha^i\epsilon_\beta^i)$ and $(\delta_\alpha^i\delta_\beta^i)$ are sufficiently small, (13) can be convexly approximated to a linear programming (LP) constraint [32] as

$$\begin{aligned}&\left(\epsilon_\alpha^i-\epsilon_\beta^i\right)\left(2x_\alpha^{i-1}-2x_\beta^{i-1}\right)+\left(\delta_\alpha^i-\delta_\beta^i\right)\left(2y_\alpha^{i-1}-2y_\beta^{i-1}\right)\\&\quad+\left(x_\alpha^{i-1}-x_\beta^{i-1}\right)^2+\left(y_\alpha^{i-1}-y_\beta^{i-1}\right)^2\geq d_{\min}^2. \quad (14)\end{aligned}$$

Note that it is also possible to modify this constraint to define an elliptical keep-out region that may have unequal dimensions in horizontal and vertical axes, which will be useful in the case of having subarrays as the smallest moving blocks instead of single antenna elements.

Finally, if the aperture size is limited, an additional condition should be forced on the element positions at each iteration so that no element can go beyond the pre-defined aperture region. Assuming a square aperture with maximum edge length $L_{\max}$, this condition is represented by

$$|\boldsymbol{x}^{i-1}+\boldsymbol{\epsilon}^i|\leq L_{\max}/2,\quad |\boldsymbol{y}^{i-1}+\boldsymbol{\delta}^i|\leq L_{\max}/2. \quad (15)$$

Overall, the convex problem to be solved at the ith iteration of the algorithm is formulated as follows:

$$\min_{\boldsymbol{\epsilon}^i,\boldsymbol{\delta}^i} \rho, \quad s.t. \quad \begin{cases} \max \left| f_{\boldsymbol{\epsilon}^i,\boldsymbol{\delta}^i}^{i,\boldsymbol{u_s},\boldsymbol{v_s}}((\boldsymbol{U},\boldsymbol{V_{SL,s}}) \right| \leq \rho \\ |\boldsymbol{\epsilon}^i| \leq \mu, \quad |\boldsymbol{\delta}^i| \leq \mu \\ (14), (15) \text{ hold for } \forall(\alpha,\beta) \end{cases} \tag{16}$$

where ρ is the maximum SLL which is simultaneously minimized for all the defined scan angles, $\boldsymbol{u_s}, \boldsymbol{v_s}$. $|\boldsymbol{\epsilon}^i|$ and $|\boldsymbol{\delta}^i|$ are upper-bounded by a user-defined constant μ, as in (4). The last two constraints guarantee that the minimum inter-element spacing at each iteration is larger than or equal to a desired value, $d_{\min}$, and the maximum aperture size is limited to $L_{\max} \times L_{\max}$.

The optimization problem presented in (16) is a nonlinear convex problem, namely a second-order cone program [32], which can be efficiently solved using interior point methods by available solvers such as CVX [33].

III. Synthesis Results

The algorithm is tested for a study case using a 64 element array ($N = 64$) with a minimum inter-element spacing $d_{\min}$. A regularly spaced array (with spacing also equal to $d_{\min}$) is used at the algorithm input and an isolated element pattern $E(\theta, \phi) = \sqrt{\cos(\theta)}$ is assumed. At this point, it is worth to mention that the square equispaced layout, that is used as the benchmark initial array topology in this article, has an impact on the optimized topologies. However, as stated in [31], the effect of using different starting element positions on the final results can be investigated by the interested users simply by modifying the element locations at algorithm initialization.

The MBO is performed for the broadside beam ($u_{s_1} = v_{s_1} = 0$) and five other beam positions ($u_{s_2} = -\sin(\pi/4)$, $v_{s_2} = -\sin(\pi/9)$, $u_{s_3} = 0$, $v_{s_3} = -\sin(\pi/9)$, $u_{s_4} = \sin(\pi/4)$, $v_{s_4} = -\sin(\pi/9)$, $u_{s_5} = -\sin(\pi/4)$, $v_{s_5} = 0$, $u_{s_6} = \sin(\pi/4)$, $v_{s_6} = 0$), covering a sector defined by a 20° range in elevation below horizon (where, statistically, almost all the ground users are located for the base station towers at relatively large heights) and a 90° azimuth coverage. The uv plane is discretized in steps of 0.01. The upper bound for the position shifts $\mu = 0.08\lambda$ is used since it has been experimentally noticed that it provides a stable convergence in a reasonable time with small transient oscillations.

The initial settings $d_{\min} = 0.5\lambda$ and $r_b = 0.28$ are used. Two cases are studied: with a constraint on the aperture size ($L_{\max} = 4\lambda$, corresponding to the standard heatsink baseplate dimensions of the commercially available CPU coolers at frequencies around 30 GHz) and without (no $L_{\max}$). Fig. 4 shows the element locations of the initial regular array and the final optimized arrays. The convergence of the maximum SLLs are shown in Fig. 5, together with the cell sector.

Figs. 6–8 provide the multi-beam radiation patterns when the beam is at broadside and is scanned toward the sector edges, in the case of the regular array, optimized array with $L_{\max} = 4\lambda$ and optimized array with no $L_{\max}$, respectively. It is seen that the optimized arrays provide 9.9 and 8.5 dB reduction in the maximum SLL for no $L_{\max}$ and $L_{\max} = 4\lambda$, respectively, when the beam is freely scanned inside the

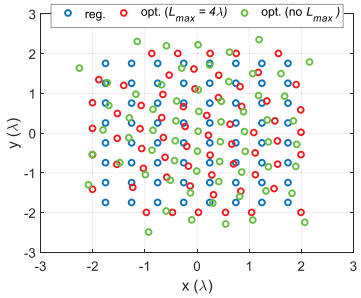

Fig. 4. Antenna locations for the test case ($N = 64$, $d_{\min} = 0.5\lambda$, $r_b = 0.28$, and $\mu = 0.08\lambda$).

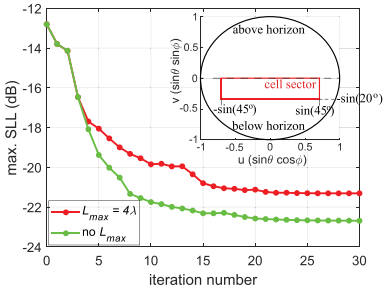

Fig. 5. Convergence of the maximum SLL for the test case ($N = 64$, $d_{\min} = 0.5\lambda$, $r_b = 0.28$, and $\mu = 0.08\lambda$) in the sector defined by a 20° range in elevation below horizon and a 90° range in azimuth.

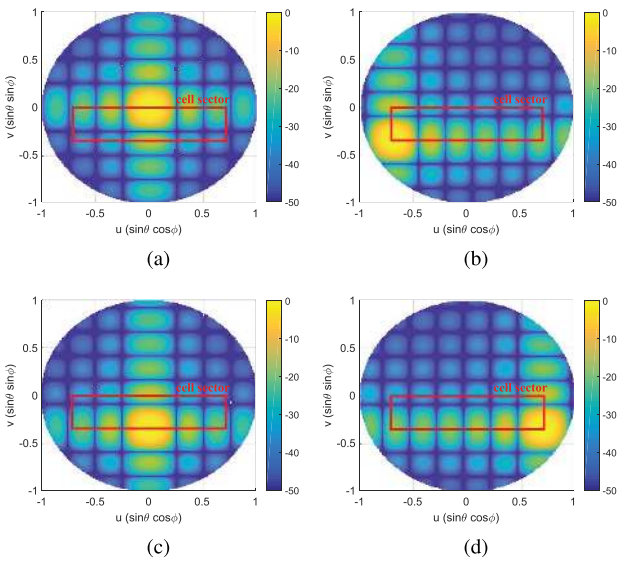

Fig. 6. Multi-beam radiation patterns (in dB, normalized) for the test case with the regular array for a beam scanned toward (a) $u_{s_1} = v_{s_1} = 0$, (b) $u_{s_2} = -\sin(\pi/4)$, $v_{s_2} = -\sin(\pi/9)$, (c) $u_{s_3} = 0$, $v_{s_3} = -\sin(\pi/9)$, and (d) $u_{s_4} = \sin(\pi/4)$, $v_{s_4} = -\sin(\pi/9)$.

defined sector. The improvement in SLLs causes an increase in the aperture size in each dimension (14.3% for $L_{\max} = 4\lambda$) when compared to the regular array with 0.5λ spacing.

All numerical computations for the synthesized 64-element arrays have been carried out on an Intel(R) Core(TM) i7-4710HQ 2.5 GHz CPU, 16 GB RAM computer using MATLAB and CVX. Each iteration takes about two hours. The simulation time mainly depends on the number of elements,

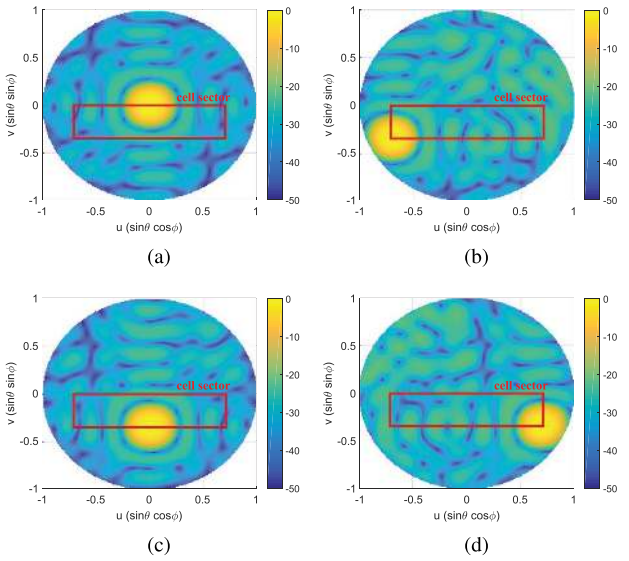

Fig. 7. Multi-beam radiation patterns (in dB, normalized) for the test case with the optimized array with $L_{\max} = 4\lambda$ for a beam scanned toward (a) $u_{s_1} = v_{s_1} = 0$, (b) $u_{s_2} = -\sin(\pi/4)$, $v_{s_2} = -\sin(\pi/9)$, (c) $u_{s_3} = 0$, $v_{s_3} = -\sin(\pi/9)$, and (d) $u_{s_4} = \sin(\pi/4)$, $v_{s_4} = -\sin(\pi/9)$.

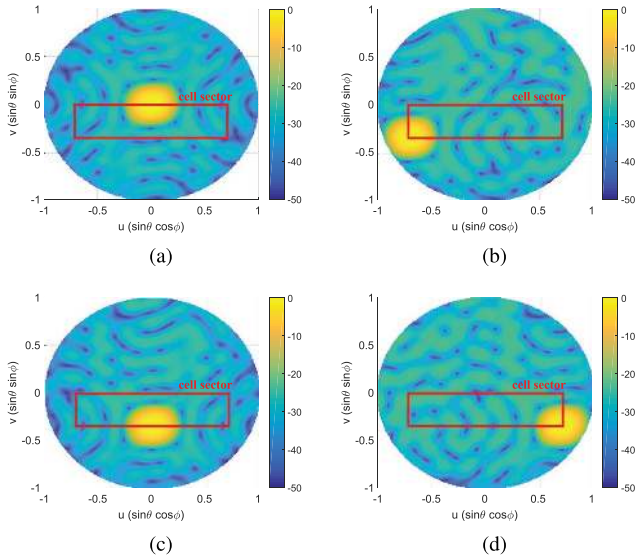

Fig. 8. Multi-beam radiation patterns (in dB, normalized) for the test case with the optimized array with no $L_{\max}$ for a beam scanned toward (a) $u_{s_1} = v_{s_1} = 0$, (b) $u_{s_2} = -\sin(\pi/4)$, $v_{s_2} = -\sin(\pi/9)$, (c) $u_{s_3} = 0$, $v_{s_3} = -\sin(\pi/9)$, and (d) $u_{s_4} = \sin(\pi/4)$, $v_{s_4} = -\sin(\pi/9)$.

the number of scan directions that is used in simultaneous MBO, the step size in the uv plane grid and if applied, the forced symmetry order in the layout.

In order to see the effect of MC on the radiation patterns, full-wave EM simulation results for the optimized layout with $d_{\min} = 0.5\lambda$ and $L_{\max} = 4\lambda$ are provided in Fig. 9. The simulations have been performed in CST Microwave Studio (MWS) for a pin-fed microstrip patch antenna array operating at the center frequency of 28.5 GHz with the patch length and width equal to 0.3λ, where λ is the free space wavelength at the center frequency, on a 0.508 mm thick substrate with $\epsilon_r = 2.2$. A square aperture is used with an

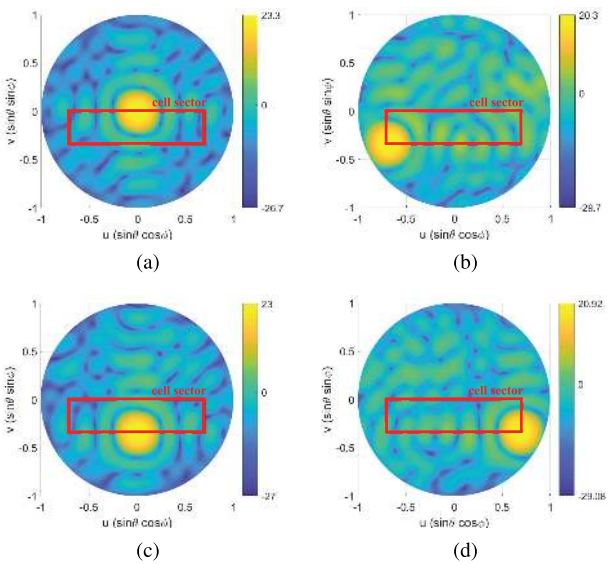

Fig. 9. Full-wave simulation multi-beam realized gain patterns for the test case with the optimized array with $L_{\max} = 4\lambda$ for a beam scanned toward (a) $u_{s_1} = v_{s_1} = 0$, (b) $u_{s_2} = -\sin(\pi/4)$, $v_{s_2} = -\sin(\pi/9)$, (c) $u_{s_3} = 0$, $v_{s_3} = -\sin(\pi/9)$, and (d) $u_{s_4} = \sin(\pi/4)$, $v_{s_4} = -\sin(\pi/9)$.

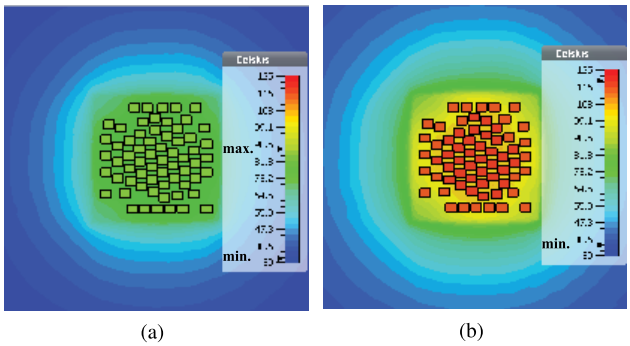

Fig. 10. Thermal simulation results for the optimized integrated array with $L_{\max} = 4\lambda$ with a passive CPU cooler having a heat transfer coefficient of 3000 W/m^{2}K, in the case of (a) 2 W and (b) 3 W heat dissipation per chip.

edge length equal to 5λ. It is seen that due to the relatively high MC (up to -13 dB), the radiation patterns given in Fig. 7 are modified and the maximum SLL increases up to -18 dB, which is seen on a circle around the main lobe. This analysis shows that, to have a better accuracy in the optimization results, either embedded element patterns should be used at each iteration of the algorithm, as done in [24] and [34]-[36], at the expense of increased optimization times and resources or MC reduction techniques, such as [37]–[39], should be exploited in the antenna design.

Using the thermal model and settings in [9], thermal simulations are also performed in CST multiphysics studio (MPS) for the optimized integrated array with $L_{\max} = 4\lambda$ with a passive CPU cooler (having a heat transfer coefficient of 3000 W/m^{2}K) attached to the beamforming chips. It is assumed that each antenna element is fed by a separate chip placed at the same 2-D location with the antenna element but on the opposite side of the substrate. The results for

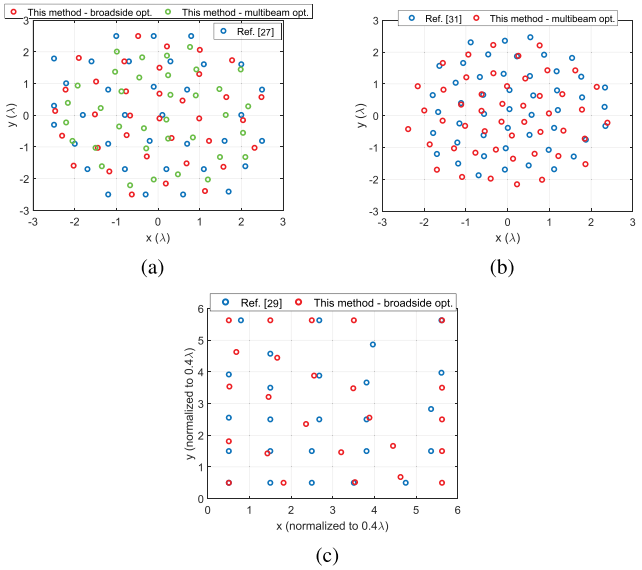

Fig. 11. Antenna locations obtained using the proposed algorithm and locations in (a) [27], (b) [31], and (c) [29].

two different relatively large heat power dissipation per chip levels (2 and 3 W) are presented in Fig. 10. It can be observed that the maximum array temperature can be kept below 90°C and 120°C even for 2 and 3 W heat dissipation per element, respectively, for an ambient temperature of 25°C, while preserving the advantage of interference suppression (see Fig. 7).

Next, the effectiveness of the proposed method is shown by adjusting the optimization parameters considering the results reported in [27], [29], and [31] and comparing the outcomes. The performance metrics used for the comparison are directivity, maximum SLL, dynamic range of excitation amplitudes and beam collection efficiency (BCE) which, according to [40], can be expressed as

$$\text{Directivity} \quad (\text{dB}) = 10lg\frac{\max_{u,v}|f(u,v)|^2}{\int_\Gamma |f(u,v)|^2 dudv} \tag{17}$$

$$\text{Max. SLL} \quad (\text{dB}) = 10lg\frac{\max_{u,v\notin\Omega}|f(u,v)|^2}{\max_{u,v}|f(u,v)|^2} \tag{18}$$

$$\text{BCE} = \frac{P_\Omega}{P_\Gamma} = \frac{\int_\Omega |f(u,v)|^2 dudv}{\int_\Gamma |f(u,v)|^2 dudv} \tag{19}$$

where P_Ω and P_Γ denote the power radiated over the angular rectenna region Ω and the total transmitted power over the whole visible space Γ, respectively. Amplitude dynamic range is the range between the smallest and largest output levels of the amplifiers feeding the elements.

In [27], a 35-element array with isotropic elements was synthesized with $d_{\min} = 0.6\lambda$ and $L_{\max} = 5\lambda$. Both element positions and excitation weights were optimized for the broadside beam, which resulted in 8.01 dB dynamic range in weights. Here, only the element positions in a uniformly excited 35-element array are optimized using the same constraints in [27] for the broadside beam and for multiple beams (broadside and scanned toward $u_s = v_s = 0.5$ to show the superiority of the algorithm). The resulting element locations

TABLE II

COMPARISON OF THE DIRECTIVITY, MAX. SLL, AMPLITUDE RANGE, AND BCE OBTAINED USING THE PROPOSED ALGORITHM WITH [27]

	Ref. [27]	This method -broadside opt.-	This method -multibeam opt.-
Directivity (dB) -broadside-	12.46	12.84	11.03
Directivity (dB) -scanned (u_s=v_s=0.5)-	9.48	9.89	10.88
Max. SLL (dB) -broadside-	-17.50	-19.51	-15.43
Max. SLL (dB) -scanned (u_s=v_s=0.5)-	-1.30	-5.50	-15.43
Excitation amplitude range (dB)	8.01	0	0
Min. inter-element spacing (λ)	0.60	0.60	0.60
BCE (%) -broadside-	54.91	68.96	52.02
BCE (%) -scanned (u_s=v_s=0.5)-	27.68	34.99	50.23

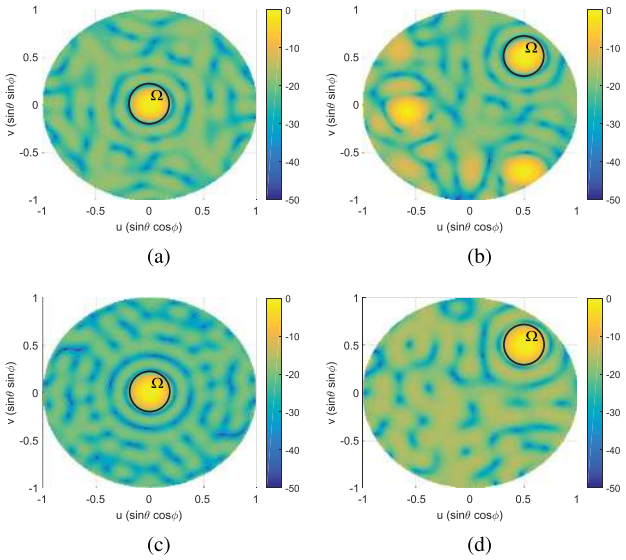

Fig. 12. Radiation patterns (in dB, normalized) for the proposed algorithm and the method in [27]. (a) From [27], broadside. (b) From [27], scanned toward $u_s = v_s = 0.5$. (c) Proposed method, broadside. (d) Proposed method, scanned toward $u_s = v_s = 0.5$.

are given in Fig. 11(a). Fig. 12 provides the corresponding radiation patterns (a circular rectenna region Ω with radius $r_b = 0.2$ is defined for BCE calculations). Comparison of results is shown in Table II. It is seen that the broadside optimization with the proposed method yields increased directivity, decreased maximum SLL and increased BCE. It is also seen that since the optimization in [27] was performed only for broadside radiation, scanning the beam leads to the formation of grating lobes in the visible region, which decreases the BCE significantly. However, the proposed MBO approach is able to guarantee low side lobes, and thus much better BCE, for both the broadside and the scanned beam simultaneously.

In [31], a 48-element patch antenna array was synthesized to achieve less than -20 dB SLL outside a circular main beam region, Ω, which is defined by a radius of $r_b = 0.25$. Element positions and excitation weights were optimized for the broadside beam and the beam scanned toward $u_s = 0.5$, $v_s = 0$, which resulted in a 6.90 dB dynamic range in weights.

TABLE III

COMPARISON OF THE DIRECTIVITY, MAX. SLL, AMPLITUDE RANGE, AND BCE OBTAINED USING THE PROPOSED ALGORITHM WITH [31]

	Ref. [31]	This method -multibeam opt.-
Directivity (dB) -broadside-	12.36	12.80
Directivity (dB) -scanned (u_s=0.5, v_s=0)-	12.28	12.72
Max. SLL (dB) -broadside-	-22.13	-23.73
Max. SLL (dB) -scanned (u_s=0.5, v_s=0)-	-21.19	-23.07
Excitation amplitude range (dB)	6.90	0
Min. inter-element spacing (λ)	0.53	0.50
BCE (%) -broadside-	88.70	91.17
BCE (%) -scanned (u_s=0.5, v_s=0)-	86.44	88.97

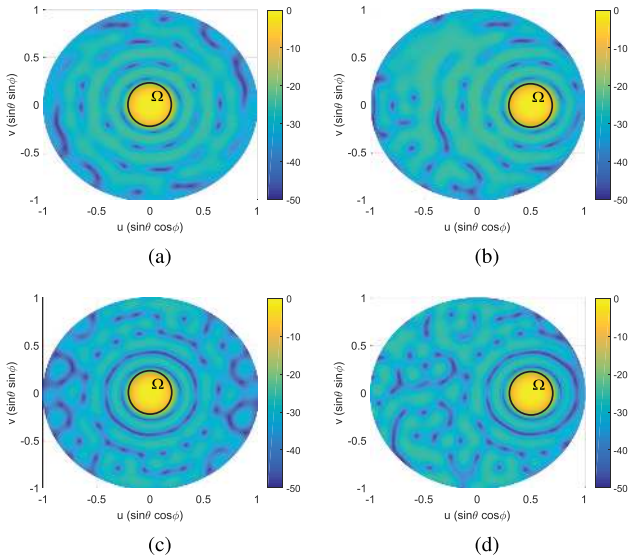

Fig. 13. Radiation patterns (in dB, normalized) for the proposed algorithm and the method in [31]. (a) From [31], broadside. (b) From [31], scanned toward $u_s = 0.5$, $v_s = 0$. (c) Proposed method, broadside. (d) Proposed method, scanned toward $u_s = 0.5$, $v_s = 0$.

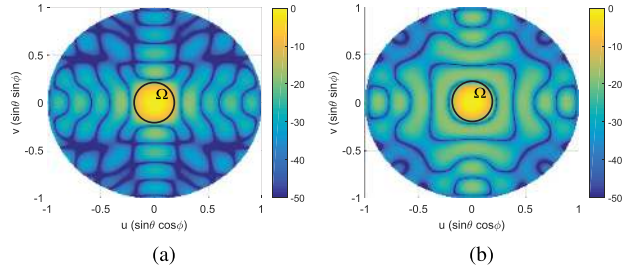

Fig. 14. Broadside radiation patterns (in dB, normalized) for the proposed algorithm and the method in [29]. (a) From [29]. (b) Proposed method.

Here, using the proposed MBO method, a new, uniformly-fed 48-element array is synthesized in order to minimize the maximum SLL while using the same settings with [31]. The resulting element locations are given in Fig. 11(b). Fig. 13 shows the corresponding radiation patterns. Comparison of results is summarized in Table III. It is seen that the proposed method is able to provide improved directivity, max. SLL and BCE for both the broadside and scanned beam, while increasing the power-efficiency by equi-amplitude excitations.

TABLE IV

COMPARISON OF THE DIRECTIVITY, MAX. SLL AND BCE OBTAINED USING THE PROPOSED ALGORITHM WITH [29]

	Ref. [29]	This method -broadside opt.-
Directivity (dB)	13.45	13.49
Max. SLL (dB)	-12.30	-18.29
Excitation amplitude range (dB)	0	0
Min. inter-element spacing (λ)	0.40	0.40
BCE (%)	89.96	79.93

In [29], the work in [40] was improved by synthesizing a uniformly-fed 100 element array while limiting the maximum SLL and maximizing the BCE in a circular rectenna region Ω with radius 0.2. It was given that $d_{\min} = 0.4\lambda$ and $L_{\max} = 4.5\lambda$. Positions of 25 elements were optimized in the first quadrant and symmetry about the x-axis and y-axis was assumed. The resulting element locations in [29] and locations given by the proposed method are shown in Fig. 11(c). Fig. 14 provides the radiation patterns at broadside for the both methods. The performance comparison is given in Table IV. It is seen that the maximum SLL can be reduced by the proposed method while keeping the same directivity. Hence, the interference among the users located at these side lobes and the main lobe becomes lower. However, due to the increase in the average level of side lobes, BCE is lower for the proposed method. In other words, the proposed algorithm yields a lower maximum SLL, but the number of side lobes reaching this maximum value is larger. Therefore, the selection between these two methods depends on the particular system requirements.

IV. CONCLUSION

A novel, system-driven array layout synthesis technique has been proposed for multi-beam phased arrays that are suitable for mm-wave 5G base station applications in simultaneous multi-user scenarios. The proposed technique achieves the optimal statistical system performance within a cell sector, while approaching the thermal management issue in the active inteagrated antenna arrays in a systematic way.

The presented algorithm combines multiple system-related issues in a single optimization procedure with low analytical complexity, compactness and easy solvability. It is based on an efficient iterative convex optimization scheme with joint capabilities, namely: 1) minimized maximum SLL everywhere in the field of view for a beam scanned freely inside a given cell sector, which creates the interference-awareness and with 2) uniform excitation amplitudes for optimum power efficiency; 3) a restricted aperture size for direct integration with the existing passive cooling systems; 4) a pre-defined minimum inter-element spacing to prevent element overlapping and ease the thermal problem caused by the temperature increase due to the too-close elements; and 5) an increased

layout sparsity via irregularity to obtain further passive cooling, which imply the thermal-awareness.

The proposed method has been applied for the synthesis of a 64 element active integrated array to be used in a cell sector defined by a scan range of 20° in elevation below horizon and 90° in azimuth. From the simulation results, it has been observed that SLLs lower than −20 dB can be achieved in the field of view while operating the array at a reliable temperature level by making use of the commercially available passive CPU coolers.

The algorithm's superior performance in comparison with the state-of-the-art methods (see [19]–[24], [27]–[31]) has also been demonstrated both qualitatively and quantitatively.

Full-wave EM simulations have shown that high MC levels may affect the radiation performance and lead to unreliable optimization results. In such cases, either MC reduction techniques can be exploited in the antenna design or embedded radiation patterns can be straightforwardly integrated into the proposed optimization procedure at the cost of increased computation time and resources.

REFERENCES

[1] J. Thompson *et al.*, "5G wireless communication systems: Prospects and challenges part 1," *IEEE Commun. Mag.*, vol. 52, no. 2, pp. 62–64, Feb. 2014.

[2] J. Thompson *et al.*, "5G wireless communication systems: Prospects and challenges part 2," *IEEE Commun. Mag.*, vol. 52, no. 5, pp. 24–26, May 2014.

[3] S. Rangan, T. S. Rappaport, and E. Erkip, "Millimeter-wave cellular wireless networks: Potentials and challenges," *Proc. IEEE*, vol. 102, no. 3, pp. 366–385, Mar. 2014.

[4] B. Hanafi, "Design of silicon power ampliers and arrays for millimeter wave applications," Ph.D. dissertation, Dept. Elect. Eng., Univ. California, San Diego, CA, USA, 2014.

[5] S. Shakib, H.-C. Park, J. Dunworth, V. Aparin, and K. Entesari, "A 28 GHz efficient linear power amplifier for 5G phased arrays in 28 nm bulk CMOS," in *IEEE Int. Solid-State Circuits Conf. (ISSCC) Dig. Tech. Papers*, San Francisco, CA, USA, Feb. 2016, pp. 3020–3036.

[6] B. J. Döring, "Cooling system for a Ka band transmit antenna array," German Aerosp. Center (DLR), Köln, Germany, Tech. Rep. IB554-06/02, Dec. 2005.

[7] Y. Aslan, J. Puskely, and A. Yarovoy, "Heat source layout optimization for two-dimensional heat conduction using iterative reweighted L1-norm convex minimization," *Int. J. Heat Mass Transf.*, vol. 122, pp. 432–441, Jul. 2018.

[8] E. McCune, "Energy efficiency maxima for wireless communications: 5G, IoT, and massive MIMO," in *Proc. IEEE CICC*, Austin, TX, USA, Apr./May 2017, pp. 1–8.

[9] Y. Aslan, J. Puskely, J. H. J. Janssen, M. Geurts, A. Roederer, and A. Yarovoy, "Thermal-aware synthesis of 5G base station antenna arrays: An overview and a sparsity-based approach," *IEEE Access*, vol. 6, no. 1, pp. 58868–58882, Oct. 2018.

[10] *Two-Resistor Compact Thermal Model Guideline*, document JESD-1, JEDEC, Jul. 2008.

[11] *Mugen MAX CPU Cooler SCMGD-1000, User Manual*, Scythe EU GmbH, Oststeinbek, Germany, Jul. 2014.

[12] D.-H. Cho *et al.*, "Beam division multiple access system and method for mobile communication system," U.S. Patent 20 100 165 914, Jul. 1, 2010.

[13] B. Sadhu *et al.*, "A 28 GHz 32-element phased array transceiver IC with concurrent dual polarized beams and 1.4 degree beam-steering resolution for 5G communication," in *IEEE Int. Solid-State Circuits Conf. (ISSCC) Dig. Tech. Papers*, San Francisco, CA, USA, Feb. 2017, pp. 128–129.

[14] R. Valkonen, "Compact 28-GHz phased array antenna for 5G access," in *IEEE MTT-S Int. Microw. Symp. Dig.*, Philadelphia, PA, USA, Jun. 2018, pp. 1334–1337.

[15] E. Degirmenci, "EMF test report: Ericsson AIR 5121," Ericsson AB, Stockholm, Sweden, Tech. Rep. GFTB-17:001589, Jan. 2018.

[16] Y. Aslan, C. E. Kiper, A. J. van den Biggelaar, U. Johannsen, and A. Yarovoy, "Passive cooling of mm-wave active integrated 5G base station antennas using CPU heatsinks," in *Proc. 16th EuRAD*, Paris, France, Oct. 2019, pp. 121–124.

[17] G. Toso, P. Angeletti, and C. Mangenot, "A comparison of density and amplitude tapering for transmit active arrays," in *Proc. 3rd EuCAP*, Berlin, Germany, Mar. 2009, pp. 840–843.

[18] R. L. Haupt, "Thinned arrays using genetic algorithms," *IEEE Trans. Antennas Propag.*, vol. 42, no. 7, pp. 993–999, Jul. 1994.

[19] D. G. Kurup, M. Himdi, and A. Rydberg, "Synthesis of uniform amplitude unequally spaced antenna arrays using the differential evolution algorithm," *IEEE Trans. Antennas Propag.*, vol. 51, no. 9, pp. 2210–2217, Sep. 2003.

[20] L. Cen, L. Y. Zhu, W. Ser, and W. Cen, "Linear aperiodic array synthesis using an improved genetic algorithm," *IEEE Trans. Antennas Propag.*, vol. 60, no. 2, pp. 895–902, Feb. 2012.

[21] O. M. Bucci, M. D'Urso, T. Isernia, P. Angeletti, and G. Toso, "Deterministic synthesis of uniform amplitude sparse arrays via new density taper techniques," *IEEE Trans. Antennas Propag.*, vol. 58, no. 6, pp. 1949–1958, Jun. 2010.

[22] J. L. Araque Quijano, M. Righero, and G. Vecchi, "Sparse 2-D array placement for arbitrary pattern mask and with excitation constraints: A simple deterministic approach," *IEEE Trans. Antennas Propag.*, vol. 62, no. 4, pp. 1652–1662, Apr. 2014.

[23] B. Fuchs, A. Skrivervik, and J. R. Mosig, "Synthesis of uniform amplitude focused beam arrays," *IEEE Antennas Wireless Propag. Lett.*, vol. 11, pp. 1178–1181, 2012.

[24] H. B. Van, S. N. Jha, and C. Craeye, "Fast full-wave synthesis of printed antenna arrays including mutual coupling," *IEEE Trans. Antennas Propag.*, vol. 64, no. 12, pp. 5163–5171, Dec. 2016.

[25] Y. Aslan, J. Puskely, A. Roederer, and A. Yarovoy, "Synthesis of multiple beam linear arrays with uniform amplitudes," in *Proc. 12th EuCAP*, London, U.K., Apr. 2018.

[26] S. E. Nai, W. Ser, Z. L. Yu, and H. Chen, "Beampattern synthesis for linear and planar arrays with antenna selection by convex optimization," *IEEE Trans. Antennas Propag.*, vol. 58, no. 12, pp. 3923–3930, Dec. 2010.

[27] M. D'Urso, G. Prisco, and R. M. Tumolo, "Maximally sparse, steerable, and nonsuperdirective array antennas via convex optimizations," *IEEE Trans. Antennas Propag.*, vol. 64, no. 9, pp. 3840–3849, Sep. 2016.

[28] C. Yan, P. Yang, and S. Y. Huang, "Synthesis of planar sparse arrays with minimum spacing constraint," *IEEE Antennas Wireless Propag. Lett.*, vol. 17, pp. 1095–1098, Jun. 2018.

[29] X. Li, B. Duan, J. Zhou, L. Song, and Y. Zhang, "Planar array synthesis for optimal microwave power transmission with multiple constraints," *IEEE Antennas Wireless Propag. Lett.*, vol. 16, pp. 70–73, Apr. 2016.

[30] C. Bencivenni, M. V. Ivashina, R. Maaskant, and J. Wettergren, "Synthesis of maximally sparse arrays using compressive sensing and full-wave analysis for global earth coverage applications," *IEEE Trans. Antennas Propag.*, vol. 64, no. 11, pp. 4872–4877, Nov. 2016.

[31] D. Pinchera, M. D. Migliore, and G. Panariello, "Synthesis of large sparse arrays using IDEA (inflating-deflating exploration algorithm)," *IEEE Trans. Antennas Propag.*, vol. 66, no. 9, pp. 4658–4668, Sep. 2018.

[32] M. S. Lobo, L. Vandenberghe, S. Boyd, and H. Lebret, "Applications of second-order cone programming," *Linear Algebra Appl.*, vol. 284, nos. 1–3, pp. 193–228, Nov. 1998.

[33] M. Grant and S. Boyd. (Mar. 2014). CVX: MATLAB software for disciplined convex programming, version 2.1. [Online]. Available: http://cvxr.com/cvx

[34] C. Bencivenni, M. V. Ivashina, R. Maaskant, and J. Wettergren, "Design of maximally sparse antenna arrays in the presence of mutual coupling," *IEEE Antennas Wireless Propag. Lett.*, vol. 14, pp. 159–162, Sep. 2014.

[35] H. B. Van, S. N. Jha, and C. Craeye, "Efficient array synthesis of printed arrays including mutual coupling," in *Proc. 10th EuCAP*, Davos, Switzerland, Apr. 2016.

[36] J. I. Echeveste, M. Á. G. de Aza, J. Rubio, and C. Craeye, "Gradient-based aperiodic array synthesis of real arrays with uniform amplitude excitation including mutual coupling," *IEEE Trans. Antennas Propag.*, vol. 65, no. 2, pp. 541–551, Feb. 2017.

[37] C.-Y. Chiu, C.-H. Cheng, R. D. Murch, and C. R. Rowell, "Reduction of mutual coupling between closely-packed antenna elements," *IEEE Trans. Antennas Propag.*, vol. 55, no. 6, pp. 1732–1738, Jun. 2007.

[38] E. Rajo-Iglesias, Ó. Quevedo-Teruel, and L. Inclan-Sanchez, "Mutual coupling reduction in patch antenna arrays by using a planar EBG structure and a multilayer dielectric substrate," *IEEE Trans. Antennas Propag.*, vol. 56, no. 6, pp. 1648–1655, Jun. 2008.

[39] Y. Aslan and A. Yarovoy, "Reduction of mutual coupling between closely spaced patch antennas using dielectric stratification technique," in *Proc. 47th EuMC*, Nuremberg, Germany, Oct. 2017, pp. 248–251.
[40] G. Oliveri, L. Poli, and A. Massa, "Maximum efficiency beam synthesis of radiating planar arrays for wireless power transmission," *IEEE Trans. Antennas Propag.*, vol. 61, no. 5, pp. 2490–2499, May 2013.

Yanki Aslan (GS'18) was born in Ankara, Turkey, in 1991. He received the B.Sc. degree, with double specialization in communications and microwaves and antennas, from the Department of Electrical and Electronic Engineering, Middle East Technical University, Ankara, Turkey, in 2014, and the M.Sc. degree *(cum laude)* in electrical engineering, telecommunications and sensing systems track from the Delft University of Technology, Delft, The Netherlands, in 2016, where he is currently pursuing the Ph.D. degree with the Microwave Sensing, Signals and Systems Group.

He is working on the project—Antenna Topologies and Front-end Configurations for Multiple Beam Generation—which is a part of STW & NXP Partnership Program on Advanced 5G Solutions. His current research interests are sparse antenna array topologies and subarrays with their beamforming architectures and requirements for 5G base stations.

Mr. Aslan was one of the recipients of the IEEE AP-S Doctoral Research Grant in 2018 and the EuMA Internship Award in 2019. He received the Justus & Louise van Effen Scholarship from the Delft University of Technology for his M.Sc. degree.

Jan Puskely was born in Prerov, Czech Republic, in 1982. He received the master's and Ph.D. degrees in electrical engineering from the Brno University of Technology (BUT), Brno, Czechia, in 2007 and 2010, respectively.

After the graduation, he worked as Post-Doctoral Researcher with the Department of Radioelectronics, BUT. He is currently a Post-Doctoral Researcher with the Microwave Sensing, Signals and Systems (MS3) Department, Delft University of Technology, Delft, The Netherlands. His current research interests include the phased antenna arrays, active and reconfigurable antenna systems, antenna array topologies, and antenna front-end designs at millimeter waves.

Antoine Roederer (LF'08) was born in Paris in 1943. He received the B.S.E.E. degree from the l'Ecole Superieure d'Electricite, Paris, France, in 1964, the M.S.E.E. degree from the University of California at Berkeley, Berkeley, CA, USA, in 1965, and the Doctorate degree (Hons.) in electrical engineering from the Universite de Paris VI, Paris, in 1972, the Honorary Doctorate degree from the Technical University of Delft, Delft, The Netherlands, 2005.

He was a Radar Antenna R&D Engineer with THOMSON-CSF, Bagneux, France, from 1968 to 1973. He joined the European Space Research and Technology Centre, ESRO (now ESA, the European Space Agency), Noordwjik, The Netherlands, in 1973, where he initiated and supervised for many years research and development and project support for space antennas. In 1993, he became the Head of the Electromagnetics Division, ESA. He is currently a part-time Scientific Advisor with the Technical University of Delft. He has authored or coauthored over 150 articles, several book chapters, and holds 20 patents in the field of antennas. This has included aspects of wideband communications, broadcasting, radar, and satellite antennas, with an emphasis on log-periodics, reflectarrays, multiple-beam reflectors and arrays, and advanced antenna feed networks. His current research interests include innovation and development in the fields of radar and 5G base station antennas.

Dr. Roederer received numerous awards for his contributions to the field of antennas and to the antenna community in Europe. He received the Fulbright Fellowship for his M.S.E.E degree. He has been the Chairman of the EU COST 260 Project on Smart Antennas. He was the Initiator and the Chairman of the Millennium Conference on Antennas and Propagation (AP 2000), Davos, precursor of the large EUCAP conferences. He retired from ESA in 2008.

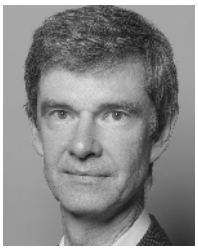

Alexander Yarovoy (F'15) received the Diploma degree (Hons.) in radiophysics and electronics and the Candidate Phys. and Math.Sci. and Doctor Phys. and Math.Sci. degrees in radiophysics from the Kharkov State University, Kharkiv, Ukraine, in 1984, 1987, and 1994, respectively.

In 1987, he joined the Department of Radiophysics, Kharkov State University, as a Researcher, where he became a Professor in 1997. From September 1994 to 1996, he was with the Technical University of Ilmenau, Ilmenau, Germany, as a Visiting Researcher. Since 1999, he has been with the Delft University of Technology, Delft, The Netherlands. Since 2009, he has been leading the Chair of Microwave Sensing, Systems and Signals. He has authored or coauthored more than 450 scientific or technical articles, four patents, and 14 book chapters. His main research interests are in high-resolution radar, microwave imaging, and applied electromagnetics (in particular, UWB antennas).

Dr. Yarovoy was a recipient of the European Microwave Week Radar Award for the paper that best advances the state-of-the-art in radar technology in 2001 (together with L.P. Ligthart and P. van Genderen) and in 2012 (together with T. Savelyev). In 2010, together with D. Caratelli, he received the Best Paper Award of the Applied Computational Electromagnetic Society (ACES). He served as the Chair and the TPC Chair of the Fifth European Radar Conference (EuRAD'08), Amsterdam, The Netherlands, and the Secretary of the First European Radar Conference (EuRAD'04), Amsterdam. He also served as the Co-Chair and the TPC Chair of the Xth International Conference on GPR (GPR2004), Delft. From 2008 to 2017, he served as the Director of the European Microwave Association (EuMA). He served as a Guest Editor of five special issues of the IEEE TRANSACTIONS and other journals. Since 2011, he has been an Associate Editor of the *International Journal of Microwave and Wireless Technologies*.